DALTON
FULL PAPER

Synthesis, spectral and redox properties of tetraammine dioxolene ruthenium complexes †

Roberto Santana da Silva,[a,b] Sergey I. Gorelsky,[a] Elaine S. Dodsworth,[a] Elia Tfouni[c] and A. B. P. Lever *[a]

[a] *Department of Chemistry, York University, 4700 Keele St., Toronto, Ontario, M3J 1P3, Canada*
[b] *Faculdade de Ciências Farmacêuticas de Ribeirão Preto, Universidade de São Paulo Av. do Café, S/N, 14040-901 Ribeirão Preto, São Paulo, Brazil*
[c] *Departamento de Quimica Faculdade de Filosofia, Ciências e Letras de Ribeirão Preto, Universidade de São Paulo Av. dos Bandeirantes, 3900, 14040-901 Ribeirão Preto São Paulo, Brazil*

Received 10th July 2000, Accepted 21st September 2000
First published as an Advance Article on the web 30th October 2000

A series of species $[Ru^{III}(NH_3)_4(Cat\text{-}R)]^{n+}$ have been synthesized where Cat-R is a catecholate dianion having the substituent R = CO_2^-, CO_2H, OMe or H. These so-called parent species were characterized by their electronic spectra, FTIR, mass spectrum, cyclic voltammetry and EPR. Controlled potential reduction yields $[Ru^{II}(NH_3)_4(Cat\text{-}R)]^{(n-1)+}$ while controlled potential oxidation yields $[Ru^{II}(NH_3)_4(Q\text{-}R)]^{(n+1)+}$ (Q-R = substituted quinone). Density Functional Theory (DFT) was primarily used to explore the electronic structures of these complexes. Application of the INDO semi-empirical model proved less useful. Time dependent density functional response theory was used to calculate the electronic spectra of the species with R = H. The electronic spectra of the closed shell species are well reproduced by the calculations. The physical properties of these complexes indicate a charge delocalized system reminiscent of a delocalized organic molecule. The simple valence descriptions noted above are convenient to use but do not reflect the actual electronic structure. The electronic spectra of the parent species are temperature dependent. The visible region charge transfer band shifts by about 1500 cm^{-1} to higher energy in acidic media at liquid nitrogen temperature. This is interpreted in terms of solvent effects rather than valence tautomerism. The electrochemical properties of $[Ru^{III}(NH_3)_4(Cat\text{-}R)]$, in aqueous solution, reveal the first example of a reversible and stable Ru–quinone species in that medium. The pK_a values for several dioxolene species, with R = CO_2^-, are derived from a Pourbaix diagram.

Introduction

In the recent past significant attention has been devoted to the properties of catechol and its oxidation products (semiquinone and quinone, generally referred to as "dioxolenes") as ligands with transition-metal ions.[1–26] The non-innocent character of these dioxolene ligands has often created ambiguity in assessing the oxidation state of the metal ion and catechol ligand. Members of the catechol–semiquinone–quinone redox chain have orbitals that can be close in energy to the transition-metal d orbitals generating an opportunity for considerable covalency between the redox-active metal centre and coordinated redox-active ligand.[4,7,10,12,13,17,18,23,24,26–33] One of the most intriguing aspects is the thermally driven valence tautomerism that has been observed for some complexes in solution or in the solid state.[1b–e,h,i,k,l,6,10,27–31,34–36] These species are characterized as electronically labile, and electronic degeneracy or near degeneracy leads to vibronic interactions and an appreciable sensitivity to the environment. The possibility of using these kinds of system as building blocks for molecular electronic devices[37] makes them of potential value and interesting to study.

Clarke and co-workers[38] have previously reported two ruthenium tetraammine complexes, $[Ru(NH_3)_4(Cat)]$ and $[Ru(NH_3)_4(Cat\text{-}CO_2)]$, However, only limited spectroscopic and voltammetric data were reported. In re-examining these compounds more intensively we noted some differences from this earlier work (*e.g.* in the number of observed redox processes) and have extended the series to $[Ru^{III}(NH_3)_4(Cat\text{-}R)]^{n+}$, R = H, OMe, CO_2^- or CO_2H, referred to here as the parent species. Q, Sq and Cat are used to describe the ligands in the quinone, semiquinonate(1−) and catecholate(2−) oxidation states.

Experimental

Physical data were recorded on instrumentation as follows: electronic spectra, Cary 2400 and Hewlett-Packard model 89532A; EPR spectra, at liquid nitrogen temperature, using a Bruker ESP300E X band spectrometer at a frequency of *ca*. 9.45 GHz and 1 mW power; infrared spectra, Mattson 3000 FTIR spectrometer using KBr or CsI pellets, with some data at 77 K; FAB mass spectra, Kratos Liquid Second Ray Ion Mass Spectrometer, with a caesium ion gun as bombarding source, glycerol as matrix and the results from an average of 5–9 scans. Electrochemical data were obtained by cyclic voltammetry using Princeton Applied Research Models 175 and 179 instrumentation. The electrochemical cell used was a conventional three electrode type: glassy carbon working electrode, platinum wire auxiliary electrode and AgCl–Ag

† Electronic supplementary information (ESI) available: Tables of frontier orbitals, DFT energies, symmetries and orbital mixing. HOMO and LUMO of the free quinone ligand, Pourbaix diagram of $[Ru(NH_3)_4(cat\text{-}CO_2)]$, FTIR spectrum of $[Ru(NH_3)_4(Cat)]Cl$ and cyclic voltammograms. See http://www.rsc.org/suppdata/dt/b0/b005488g/

 DOI: 10.1039/b005488g

reference electrode. The potentials were calibrated with respect to the $[Ru^{III}(NH_3)_6]^{3+}$–$[Ru^{II}(NH_3)_6]^{2+}$ couple ($E_{1/2} = 0.05$ V *vs.* SHE).[39] The pH measurements were made with a Fisher Accumet pH meter model 120. The pH was adjusted from 3.5 to 7.0 with acetate buffer and 1.8 to 3.5 with trifluoroacetate buffer. Potassium chloride was added to keep a minimum ionic strength $I = 0.2$ M. C, H, and N analysis were furnished by Guelph Chemicals Laboratories Ltd. and the University of São Paulo.

The complex $[Ru^{III}(NH_3)_5Cl]Cl_2$ was prepared using a published procedure.[40] The species $[Ru^{III}(NH_3)_6]Cl_3$, 3,4-dihydroxybenzoic acid (H_2Cat-CO_2H), 1,2-dihydroxy-4-methoxybenzene (H_2Cat-OMe) and 1,2-dihydroxybenzene (H_2Cat) were used as supplied (Aldrich). Potentially displaceable protons on the ligands are noted in the abbreviations, thus Cat-CO_2 carries three negative charges.

Preparation of complexes

All the complexes were synthesized under an argon atmosphere.

$[Ru^{III}(NH_3)_4$(Cat-CO_2)]. This complex was synthesized according to the literature method.[41] However the published elemental analysis for hydrogen was poor. We now report an improved elemental analysis. Calc. for $[Ru^{III}(NH_3)_4$(Cat-CO_2)]·$2H_2O$, $C_7H_{19}N_4O_6Ru$: C, 23.60; H, 5.37; N, 15.72. Found: C, 24.04; H, 5.31; N, 15.54%.

$[Ru^{III}(NH_3)_4$(Cat)]Cl. This complex was similarly synthesized using a solution of 1,2-dihydroxybenzene in aqueous ammonia. The ligand in excess was removed by washing 3 times with diethyl ether. Sodium chloride (0.58 g, 1×10^{-2} mol) was added to the solution. The NaCl in excess and other by-products were removed by fractional precipitation by adding acetone (150 ml). The complex $[Ru^{III}(NH_3)_4$(Cat)]Cl was separated by filtration after standing for 5 h in a freezer and washed three times with ethanol–water (90 : 10 v/v). Yield 40%. Calc. for $[Ru^{III}(NH_3)_4$(Cat)]Cl·$2H_2O$, $C_6H_{20}ClN_4O_4Ru$: C, 20.66; H, 5.78; N, 16.07. Found: C, 21.00; H, 5.04; N, 16.00%. The mass spectrum showed peaks at *m*/*z* 278(P) and at 261, 244 and 227 due to successive loss of NH_3.

$[Ru^{III}(NH_3)_4$(Cat-OMe)]Cl. This complex was synthesized and purified similarly to $[Ru^{III}(NH_3)_4$(Cat)]Cl, but using 1,2-dihydroxy-4-methoxybenzene as ligand. Yield 30%. Calc. for $[Ru^{III}(NH_3)_4$(Cat-OMe)]Cl·H_2O, $C_7H_{20}ClN_4O_4Ru$: C, 23.30; H, 5.59; N, 15.53. Found: C, 23.78; H, 5.02; N, 15.47%.

$[Ru^{III}(NH_3)_4$(Cat-CO_2H)]Cl. This complex was prepared by dissolution of $[Ru^{III}(NH_3)_4$(Cat-CO_2)] in HCl at pH 4.0 and evaporation to dryness.

$[Ru^{III}(ND_3)_4$(Cat-R)]$^+$ (Cat-R = Cat, Cat-OMe or Cat-CO_2D). The $[Ru^{III}(ND_3)_4$(Cat-R)] species were prepared by dissolving $[Ru^{III}(NH_3)_4$(Cat-R)]$^{n+}$ in D_2O. Sodium deuteroxide was added in order to have pD around 9.0. Higher pD must be avoided to prevent decomposition, The $[Ru^{III}(ND_3)_4$(Cat-CO_2D)]Cl was prepared similarly by addition of DCl to $[Ru^{III}(ND_3)_4$(Cat-CO_2)].

$[Ru^{II}(NH_3)_4$(Q-R)]$^{2+}$ and $[Ru^{II}(NH_3)_4$(Cat-R)] (Q-R = Q, Q-OMe or Q-CO_2H). These were synthesized *in situ* by controlled potential electrolysis, oxidation and reduction respectively.

Computational details

As a starting geometry for density functional theory (DFT) calculations we used an optimized geometry at the semi-empirical level, obtained using the INDO/1[42a] method with $\beta(d) = -14$ eV for Ru and with the overlap weighting factors

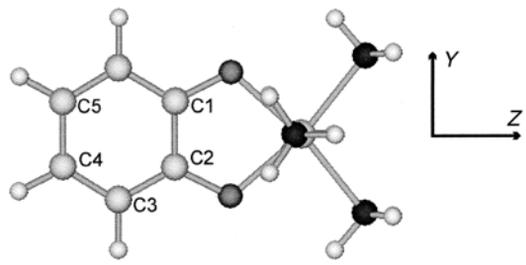

Fig. 1 Structure of the $[Ru(NH_3)_4(Cat)]$ fragment and coordinate axes.

σ–σ and π–π both set at 1.0.[42a] This was obtained using a developmental version of ZINDO kindly provided by Zerner and running on a SGI Origin 2000 Computer. INDO/S calculations used Zerner's INDO/S model with code written by Reimers and Hush[42b] and were performed on the geometry optimized structures. The overlap weighting factors σ–σ and π–π were set at 1.265 and 0.585, respectively. These programs were run on a Pentium III 600 MHz or Silicon Graphics Origin Computer.

All DFT calculations were carried out using GAUSSIAN 98.[43] We used Becke's three parameter hybrid functional[44] with LYP correlation functional[45] (B3LYP) employing an effective core potential (ECP) triple-split basis set (CEP-121G),[46] LanL2DZ ECP,[47] Stuttgart/Dresden ECP (SDD),[48] and split-valence double-zeta plus polarization orbital basis set (DZVP).[49] Basis set dimensions were 162 basis functions/414 primitive gaussians (LanL2DZ), 191/417 (SDD), 226/334 (CEP-121G) and 236/548 (DZVP).

The R = H complexes were optimized within C_{2v} symmetry. The stability of the DFT wavefunctions was tested with respect to relaxing spin and symmetry constraints. Energy minima were characterized by harmonic frequency calculations. The axis system adopted in this work is shown in Fig. 1.

Gross Mulliken populations of molecular orbitals were obtained using the program MOMIX.[50a] Time dependent density functional response theory (TD-DFRT)[51] calculations were performed on the closed shell species, wherein the energies and intensities of the lowest 30 singlet–singlet transitions were calculated.

The Onsager self consistent reaction field model (SCRF)[52] with a spherical cavity in a continuum with a dielectric constant (relative permittivity) $\varepsilon = 78.39$, corresponding to water at 298 K, was also used for modeling the interaction between the solute and the solvent. The calculated radius of the solute, $[Ru(NH_3)_4(Cat)]^+$, was 4.80 Å for B3LYP/DZVP and 4.87 Å for B3LYP/LanL2DZ calculations.

Results

Synthesis

The complexes $[Ru^{III}(NH_3)_4$(Cat-R)] (Cat-R = Cat, Cat-OMe or Cat-CO_2) have been prepared by treating $[Ru^{III}(NH_3)_5Cl]Cl_2$ with the corresponding catechol in the presence of base under an inert atmosphere. The tetraammine(R-substituted catechol ato)ruthenium(III) complexes are denoted as $[Ru^{III}(NH_3)_4$(Cat-R)]$^{n+}$ ($n = 0$ for Cat-CO_2 and 1 for Cat, Cat-OMe or Cat-CO_2H).

The anionic catechol ligands are bases (pK_a is *ca.* 9 for the first proton and *ca.* 11 for the second one).[53] As coordination to the metal involves ligand deprotonation in the first step, 7 M aqueous ammonia was used for that purpose, although Clarke and co-workers[38] used phosphate buffer solution in a similar synthesis. Phosphate buffer appears to induce some side reactions leading to a different product. The electronic spectrum of $[Ru^{III}(NH_3)_6]Cl_3$ in a phosphate buffer solution (pH 10) was compared with that in 7 M aqueous ammonia. In the first solution a new band appears around 27000 cm^{-1} which is

Table 1 Main FTIR bands of $[Ru(NH_3)_4(Cat\text{-}R)]Cl_n$ ($n = 0$ or 1) and related complexes. Data in wavenumbers collected from KBr disks

	Assignment				
Complex	δ_a(HNH)	δ_s(HNH)	$\rho_r(NH_3)$	Other	ν (diolato ring)
$[Ru^{III}(NH_3)_4(cat)]Cl$	1637 (m)	1298 (s), 1267 (s)	814 (m)	—	1568 (w), 1460 (m), 1415 (w), 1244 (m), 856 (m), 783 (m), 761 (s)
$[Ru^{III}(ND_3)_4(cat)]Cl$	1184 (mw)	993 (m)	633 (m)	—	1458 (s), 1304 (m), 1248 (s), 1103 (m), 1028 (m), 856 (m), 787 (m), 756 (s)
$[Ru^{III}(NH_3)_4(Cat\text{-}OMe)]Cl$	1622 (m)	1300 (m)	—	1088 (s)[a]	1466 (s), 1446 (m), 1242 (m), 770 (m), 723 (m)
$[Ru^{III}(ND_3)_4(Cat\text{-}OMe)]Cl$	—	1070 (m)	—	1088 (s)[a]	1570 (m), 1466 (s), 1439 (m), 1410,[a] 1242 (m), 997 (m), 769 (m), 723 (m)
$[Ru^{III}(NH_3)_4(Cat\text{-}CO_2)]$	1616 (m)	1308 (m)	823 (m)	1566 (m),[b] 1358 (s)[c]	1508 (m), 1408 (m), 1267 (s), 791 (m), 663 (mw)
$[Ru^{III}(NH_3)_4(Cat\text{-}CO_2H)]Cl$	1614 (m)	1294 (s)	812 (m)	1681 (m)[d]	1497 (w), 1448 (w), 1194 (m), 1119 (m), 1057 (m), 773 (m)
$[Ru^{III}(ND_3)_4(Cat\text{-}CO_2)]$	1185 (w)	1000 (mw)	—	1568 (m),[b] 1358 (s)[c]	1518 (m), 1456, 1404 (m), 1267 (s), 791 (m), 669 (m)
$[Ru^{III}(ND_3)_4(Cat\text{-}CO_2D)]Cl$	1117 (m)	1085 (m)	645 (m)	1671 (m),[b] 1378[c]	1575 (m), 1195 (m), 938 (w), 785 (m), 1270 (s)

w = Weak, m = medium, s = strong. [a] ν_{CO}(OMe). [b] $\nu_{asym}(CO_2^-)$. [c] $\nu_{sym}(CO_2^-)$. [d] $\nu_{asym}(CO_2H)$.

not present in the spectrum taken of the aqueous ammonia solution. Similar results were obtained by dissolving $[Ru^{III}(NH_3)_5Cl]Cl_2$ in phosphate medium. Phosphato complexes may be formed. The variation in electrochemical behavior between our $[Ru(NH_3)_4(Cat)]$ species and those of Clarke and co-workers[38] may possibly be due to the presence of some phosphate side-product. The isolated $[Ru^{III}(NH_3)_4(Cat)]Cl$, $[Ru^{III}(NH_3)_4(Cat\text{-}OMe)]Cl$ and $[Ru^{III}(NH_3)_4(Cat\text{-}CO_2)]$ are stable in air and can be stored for long periods without any change.

FTIR

The main bands in the infrared spectra of the parent $[Ru^{III}(NH_3)_4(Cat\text{-}R)]^{n+}$ species are shown in Table 1. The band assignments were facilitated by comparison with the deuteriated species. The data are consistent with the formation of a catechol species showing a strong band near 1250 cm^{-1}. However a second strong band expected near 1480 cm^{-1} was not observed.[54] Both NH_3 stretching and rocking vibrations were assigned. The NH_3 rocking vibration, whose frequency is a measure of the metal–NH_3 interaction,[55–59] was observed for $[Ru^{III}(NH_3)_4(Cat\text{-}R)]^{n+}$ near 820 cm^{-1}. This is taken as an indication of a strong interaction between Ru^{III} and NH_3 in $[Ru^{III}(NH_3)_4(Cat\text{-}R)]^{n+}$, in comparison to some other ammine complexes also shown in Table 1. This rocking vibration was generally difficult to observe in the data at room temperature, but, for the unsubstituted complex, was resolved clearly in data collected when the sample was cooled to liquid nitrogen temperature (ESI Fig. S1).

Electron paramagnetic resonance (EPR) spectra

In the solid state, at liquid nitrogen temperature, the parent complexes yield very broad and poorly resolved EPR signals which are not very satisfactory but are illustrative of a ruthenium(III)[60] contribution rather than a semiquinone free radical bound to Ru^{II}, *e.g.* see a free radical signal for a related Ru^{II}–semiquinone species (Fig. 3 in ref. 26*a*).

In frozen aqueous acidic medium (HCl–MeOH–water) these species (R = H or CO_2; OMe was not studied) generally present a narrow signal [$g \approx 2.08$, pp (peak to peak separation) ≈ 50 G] indicative of a free radical with some small ruthenium contribution. In neutral (MeOH–water) solution the signal broadens (pp ≈ 400 G) and a shift to $g \approx 2.3$ consistent with a significantly greater ruthenium(III) contribution but in no case do we observe the 3 g values typical of ruthenium(III) species.[60] No signal can be observed at room temperature. This is also consistent with the presence of Ru^{III} rather than a simple organic free radical.

Table 2 Electrochemical potentials for the parent $[Ru^{III}(NH_3)_4(Cat\text{-}R)]^+$ species, in water.[a] Volts *vs.* AgCl–Ag. Supporting electrolyte 0.1 M KCl, scan rate 0. 2 V s^{-1}

Complex	$E_{1/2}$ ($Ru^{II}(Q)$–$Ru^{III}(Cat)$)	$E_{1/2}$ ($Ru^{III}(Cat)$–$Ru^{II}(Cat)$)
$[Ru^{III}(NH_3)_4(Cat)]^+$	0.23	−0.70
$[Ru^{III}(NH_3)_4(Cat\text{-}OMe)]^+$	0.22	−0.70
$[Ru^{III}(NH_3)_4(Cat\text{-}CO_2)]^+$	0.32	−0.65

[a] See ESI Fig. S2 for an example of the cyclic voltammogram. Note that regions I, II and III in Fig. S2 refer to potentials negative of −0.70, between +0.2 and −0.65 and positive of 0.32 V respectively.

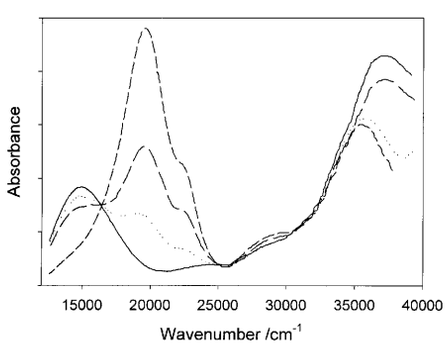

Fig. 2 Electronic spectra recorded with an optically transparent thin layer electrode (OTTLE) cell during the oxidation of 10^{-3} M $[Ru^{III}(NH_3)_4(Cat)]^+$ (as chloride, solid line) to $[Ru^{II}(NH_3)_4(Q)]^{2+}$ (final – – – line) in aqueous 0.2 M KCl.

Electrochemistry

The cyclic voltammetry (CV) data for $[Ru^{III}(NH_3)_4(Cat\text{-}R)]^+$, in aqueous solution, are listed in Table 2 and shown for $[Ru^{III}(NH_3)_4(Cat\text{-}CO_2)]$ in ESI Fig. S2. At pH 7.0 two couples were found in the region scanned (0.8 to −1.0 V *vs.* AgCl–Ag). The Nicholson–Shain[61] criteria (I_{pa} *vs.* scan rate; $I_{pa}/I_{pc} = 1$; and peak–peak separation near 60 mV) were used to diagnose the couples as reversible, one-electron processes in all three complexes.

On the basis of previous literature[12,13,17] and spectroelectrochemistry (Fig. 2) described below, the species existing in solution upon controlled potential reduction or oxidation of the parent species, $[Ru^{III}(NH_3)_4(Cat\text{-}R)]^+$ (at points I and III in Fig. S2), are formally $[Ru^{II}(NH_3)_4(Cat\text{-}R)]$ and $[Ru^{II}(NH_3)_4(Q\text{-}R)]^{2+}$ respectively.

Studying the pH dependence of the peak potentials in buffer solutions allows one to obtain the pK_a values for several

Table 3 Electronic spectral data of the $[Ru^{II}(NH_3)_4(Q\text{-}R)]$, $[Ru^{III}(NH_3)_4(Cat\text{-}R)]$ and $[Ru^{II}(NH_3)_4(Cat\text{-}R)]$ series in aqueous solution at room temperature

Observed band energy (ε, $\Delta_{1/2}$)[a]		
R = H	R = OCH_3	R = CO_2
$[Ru^{II}(NH_3)_4(Q\text{-}R)]^{2+}$ [b]		
19400 (7.6, 1870)	19600 (8.5, 2130)	19270 (7.6, 1690)
22200sh	22700sh	21900sh
27800sh	27800sh	27800sh
36750 (6.7)	37050	35200
$[Ru^{III}(NH_3)_4(Cat\text{-}R)]^{+}$		
14800 (2.9, 2730)[c]	14500 (2.9, 2630)	15200 (2.8, 2390)
24300sh[c]		
28600sh[c]		
35000 (4.8)[c]	36000sh	33700 (8.2), 37600 (9.3)
44200 (8.9)[c]	47200 (18.2)	47200 (24.1)
$[Ru^{II}(NH_3)_4(Cat\text{-}R)]$	[d]	
30700sh		35200 (12.6)
37800 (6.7)		37800 (12.8)

[a] Data are presented as energy in cm^{-1} with, in parentheses, molar absorptivity in 1000 M^{-1} cm^{-1} and half band width in cm^{-1}, only shown for bands that are well separated from other bands. [b] Data for the Q-R species were collected by spectroelectrochemistry in the presence of 0.1 M KCl. [c] ROHF INDO/S predicted electronic spectra using B3LYP/DZVP optimized geometry (prominent bands only): 14000(0.085), H-3 ⟶ S, d ⟶ π* $^2B_1$; 24350(0.04), S ⟶ L, π ⟶ π* $^2B_2$; 27400(0.002), H-1 ⟶ L + 3, d ⟶ d $^2B_1$; 33300(0.02), S ⟶ L + 2, π ⟶ π* $^2B_1$; 36650(0.07), H-8 ⟶ S, π ⟶ π* $^2A_2$; 37800(0.13), H-2 ⟶ L + 1, d ⟶ π* $^2B_1$. H = HOMO, L = LUMO, S = SOMO. [d] The UV bands for $[Ru^{II}(NH_3)_4(Cat\text{-}OMe)]$ occur below 250 nm and were not recorded.

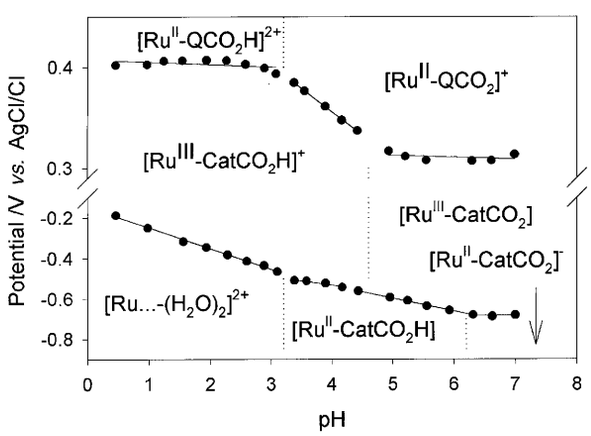

Fig. 3 The pH–potential regions of stability for the various oxidation states of the R = CO_2^- species. The species existing in each region are indicated by using, for example, abbreviations such as $[Ru^{III}\text{-}Cat\text{-}CO_2]$ for $[Ru(NH_3)_4(Cat\text{-}CO_2)]$. The p$K_a$ values are shown by the vertical lines in the various *E vs.* pH regions.

species (Fig. 3). In acidic medium below pH *ca.* 3 the fully reduced $[Ru^{II}(NH_3)_4(Cat\text{-}R)]$ species dissociate irreversibly to *cis*-$[Ru(NH_3)_4(H_2O)_2]^{2+}$ *via* a mechanism which has been discussed previously.[41]

Electronic spectra and spectroelectrochemistry

The electronic spectral data for this series of tetraammine ruthenium complexes in the three oxidation states are shown in Table 3. Fig. 3 displays the spectra of the parent $[Ru^{III}(NH_3)_4(Cat\text{-}CO_2)]$ and of $[Ru^{II}(NH_3)_4(Q\text{-}CO_2)]$ prepared by controlled potential oxidation (in region III). Controlled potential reduction of $[Ru^{III}(NH_3)_4(Cat\text{-}CO_2)]$ (in region I in ESI Fig. S2) yields a species with no strong visible region absorption consistent with its formulation as $[Ru^{II}(NH_3)_4(Cat\text{-}R)]$. The spectroelectrochemical changes are fully reversible.

Table 4 Summary of low temperature UV/Vis data (thermochromism) for $[Ru^{III}(NH_3)_4(Cat\text{-}R)]^{+}$

	MeOH–EtOH–water[a]		0.1 M HCl in MeOH–EtOH	
Cat-R	298 K	78 K	298 K[b]	78 K
Cat	13.9	15.4		
	22.9	24.4		
	27.9sh	31.1sh	15.6	17.3
	36.0	34.5		
	14.1			
Cat-OMe	32.5sh			
	37.9sh			
	46.3			
	14.5			
$Cat\text{-}CO_2$	33.3		15.6[c]	17.2[c]
	37.7			

[a] 49.7 : 49.7 : 0.6. [b] 50 : 50, with 0.1 mL conc. HCl. [c] Corresponds to $Cat\text{-}CO_2H$ species.

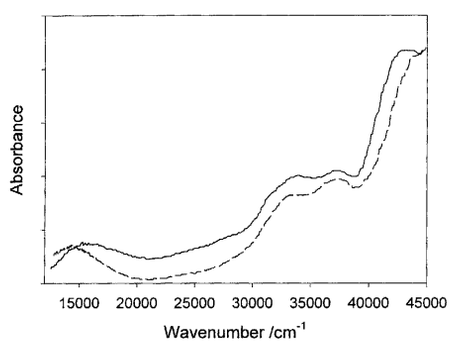

Fig. 4 Electronic spectrum of $[Ru^{III}(NH_3)_4(Cat\text{-}CO_2)]$ in EtOH–MeOH–water solution at room temperature (hatched line) and liquid nitrogen temperature (solid line).

The Ru^{II}–quinone exhibits an intense visible region band common to this type of species,[12,13,17,26] fundamentally a Ru→Q MLCT transition. The energy shifts slightly with substituent R, increasing in the sequence $CO_2^- < H < OMe$.

The parent Ru^{III}–catecholate species show a rather weaker and certainly broader, visible region band, at lower energy than the aforementioned Ru–Q transition and which also shifts slightly with R but in the opposite sense. The visible absorption spectra of these Ru^{III}–catecholate species are moderately temperature dependent as indicated in Table 4. For example, in methanol–ethanol–water (49.7 : 49.7 : 0.6) the frequency of the low energy band in the spectrum of the $[Ru^{III}(NH_3)_4(Cat\text{-}CO_2)]$ species shifts to the blue with a decrease in temperature. This shift is even more pronounced in 0.1 M HCl at cryogenic temperatures (Table 4; Fig. 4).

Geometry optimization and TD-DFRT calculations (Tables 5–11)

The geometries of the $[Ru(NH_3)_4(O_2C_6H_4)]^{2+/1+/0}$ species were optimized using DFT (B3LYP) with various basis sets for the purposes of generating input coordinates to derive electronic structural information. There are still relatively little data in the literature concerning the performance of different basis set combinations for different types of problems, including geometries, vibrational and electronic spectra of transition metal complexes. These results are listed in Tables 5–7.

B3LYP is currently the most widely used hybrid functional for studying different types of problems from geometry to thermochemistry to optical properties, *etc.*[62] In these systems it provides excellent electronic spectroscopic predictions (see below) even though the calculated Ru–N and Ru–O distances

Table 5 DFT Optimized geometries (distances in Å, angles in °) of $[Ru(NH_3)_4(O_2C_6H_4)]^{2+}$ (C_{2v}) using B3LYP

	LanL2DZ	SDD	CEP-121G	DZVP	DZVP+SCRF[a]
$Ru–N_{eq}$	2.169	2.163	2.186	2.190	2.185
$Ru–N_{ax}$	2.179	2.168	2.193	2.198	2.195
$N–Ru–N_{eq}$	97	98	97	94	93
$N–Ru–N_{ax}$	179	180	180	179	179
Ru–O	2.063	2.041	2.072	2.088	2.086
$C^1–O$	1.310	1.317	1.317	1.271	1.272
$C^1–C^2$	1.498	1.490	1.506	1.508	1.499
$C^2–C^3$	1.429	1.427	1.437	1.432	1.433
$C^3–C^4$	1.383	1.385	1.388	1.367	1.367
$C^4–C^5$	1.461	1.459	1.470	1.460	1.455

[a] The SCRF calculations (the Onsager model, solvent–water, $a_0 = 4.82$ Å).

Table 6 DFT Optimized geometries (distances in Å, angles in °) of $[Ru(NH_3)_4(O_2C_6H_4)]^{1+}$ (C_{2v}) using B3LYP[a]

	LanL2DZ	CEP-121G	DZVP	DZVP+SCRF[b]
$Ru–N_{eq}$	2.197	2.209	2.221	2.212
$Ru–N_{ax}$	2.174	2.189	2.195	2.189
$N–Ru–N_{eq}$	102	103	99	94
$N–Ru–N_{ax}$	172	172	172	176
Ru–O	2.049	2.060	2.075	2.074
$C^1–O$	1.360	1.368	1.315	1.316
$C^1–C^2$	1.449	1.456	1.457	1.448
$C^2–C^3$	1.418	1.426	1.420	1.419
$C^3–C^4$	1.397	1.402	1.382	1.387
$C^4–C^5$	1.428	1.435	1.426	1.419

[a] B3LYP/SDD optimization converges to planar $[Ru(NH_3)_2(O_2C_6H_4)]^+$ solvated by two NH_3. See Fig. 1 for labeling scheme. [b] SCRF calculations (the Onsager model, solvent–water, $a_0 = 4.80$ Å).

Table 7 DFT Optimized geometries (distances in Å, angles in °) of $[Ru(NH_3)_4(O_2C_6H_4)]$ (C_{2v}) using B3LYP[a]

	LanL2DZ	SDD	CEP-121G	DZVP	DZVP+SCRF[b]
$Ru–N_{eq}$	2.225	2.206	2.232	2.247	2.235
$Ru–N_{ax}$	2.177	2.163	2.186	2.191	2.185
$N–Ru–N_{eq}$	109	110	111	107	94
$N–Ru–N_{ax}$	163	163	163	163	169
Ru–O	2.083	2.074	2.091	2.076	2.118
$C^1–O$	1.389	1.391	1.399	1.357	1.335
$C^1–C^2$	1.445	1.444	1.450	1.438	1.451
$C^2–C^3$	1.410	1.409	1.417	1.406	1.410
$C^3–C^4$	1.412	1.412	1.418	1.404	1.411
$C^4–C^5$	1.409	1.410	1.415	1.399	1.399

[a] See Fig. 1 for labeling scheme. [b] SCRF calculations (the Onsager model, solvent–water, $a_0 = 4.82$ Å).

tend to be somewhat longer than anticipated based upon X-ray crystallographic data for related species. For example the $Ru^{III}–NH_3$ distance is expected around 2.10 Å [63] and $Ru^{II}–NH_3$ ranges experimentally between 2.10 and 2.20 Å.[64,65] The Ru–O bonds are also somewhat long as are the internal C–C and C–O dioxolene distances. These differences may partly be due to the fact that this is a "gas phase" calculation with no involvement of solvent. In a recent study of $[Ru(NH_3)_6]^{2+/3+}$ [66] it was shown that interactions with counter ions can also decrease the $Ru–NH_3$ distances by ≈0.05 Å, so that $Ru–NH_3$ distances from solid state structures may not exactly resemble those of gas phase structures.

The optimized structure of $[Ru^{II}(NH_3)_4(Q)]^{2+}$ ion shows a pseudo octahedral arrangement of ligands around the metal atom with axial and equatorial $H_3N–Ru–NH_3$ angles of 180 and 93–98°. For $[Ru^{III}(NH_3)_4(Cat)]^+$ ion the axial $H_3N–Ru–NH_3$ angle is no longer 180 but 172°. For $[Ru^{II}(NH_3)_4(Cat)]$ the distortion from the octahedral arrangement is even greater; the axial $H_3N–Ru–NH_3$ angle is 163° and equatorial $H_3N–Ru–NH_3$ angle grows to 111°. This small tilt in the axial $H_3N–Ru–NH_3$ angle is reproduced in all the calculations (and indeed appears also in INDO/1 calculations, to a lesser extent). Optimizing the structures (using DZVP) including solvent with the SCRF model [Tables 5–7] shows a smaller degree of distortion from the octahedral arrangement; the axial $H_3N–Ru–NH_3$ angle goes from 179 (2+ ion) to 169° (zero charge species) and the equatorial $H_3N–Ru–NH_3$ angle remains around 94°. Thus, the solute–solvent interaction brings the Ru–ligand angles closer to the expected octahedral values.

The calculated axial $Ru–NH_3$ distance does not significantly change in the 2+/1+/0 charged complexes, but the equatorial $Ru–NH_3$ distance tends to decrease with increasing positive charge on the complex. As a result, for $[Ru^{II}(NH_3)_4(Cat)]$ and $[Ru^{III}(NH_3)_4(Cat)]^+$ the axial $Ru–NH_3$ distance is shorter than the equatorial $Ru–NH_3$ distance, while for $[Ru^{II}(NH_3)_4(Q)]^{2+}$ the two distances are equivalent.

The most important changes in the set of $[Ru(NH_3)_4(dioxolene)]^{2+/1+/0}$ complexes are observed in the catechol/quinone ring. For the $[Ru^{II}(NH_3)_4(Q)]^{2+}$ complexes there is a clear alternation of long and short C–C bond distances consistent with a quinone structure. When the charge of the complex is reduced to +1 this alternation becomes less and at

zero charge it disappears. The C^3–C^4 and C–O bonds become longer and C^1–C^2 and C^4–C^5 bonds become shorter. The calculated C–O bond length in the 2+ species is consistent with that anticipated for, and only slightly shorter than, a bound semiquinone which is consistent with a quinone having fairly extensive back bonding. The calculated C–O bond length in the neutral reduced species agrees with that anticipated for a catecholate.[67] The C–O bond length in the 1+ is intermediate between the typical semiquinone and catechol distances.

The TD-DFRT method is gaining prominence as an accurate procedure to derive excited state transition energies.[51] The predicted electronic spectral data using the several functionals are shown in Table 8. The B3LYP functional with the DZVP basis set (using the optimized geometry at the same level) provides the best agreement with experiment (compare with data in Table 3).

In view of our previous experience using the semi-empirical INDO method,[33c,e,f,68] we did investigate using this model for these species. INDO/1 gave bond lengths significantly closer to those expected, based on literature crystal structure data of related species, than those obtained with DFT(B3LYP). However, using these geometries, the agreement between the INDO/S predicted optical spectra with experiment was decidedly inferior to the TD-DFRT results. Somewhat surprisingly, the electronic spectra predicted for both the closed shell complexes (R = H) using INDO/S with *the DFT optimized geometries* were in good agreement with experiment. Since DFT works well with these species, albeit with somewhat longer bonds, we do not report the INDO data save for the predicted INDO/S spectrum of the open shell species (R = H).

Discussion

Redox properties

The $[Ru^{III}(NH_3)_4(Cat\text{-}R)]$ species can be oxidized or reduced reversibly in one electron redox couples in aqueous solution. This is in contrast to the "free" ligand which has complicated electrochemical behavior due to coupled protonation processes.[69–72] The coordination of the catecholate ligand to ruthenium effectively decreases the pK_a of the catechol species, simplifying the electrochemical mechanism. In acidic medium (pH ≈ 3.0 depending on R) reduction of the metal center in $[Ru^{III}(NH_3)_4(Cat\text{-}R)]$ is followed by dissociation of the catecholate ligand by a fast chemical reaction.[62]

The redox couples for $[Ru^{III}(NH_3)_4(Cat\text{-}CO_2)]$ are pH-dependent, as shown in the Pourbaix diagram (Fig. 3). From these data one may conclude that the pK_a values for the carboxylic acid function of $[Ru^{II}(NH_3)_4(Cat\text{-}CO_2H)]$ and $[Ru^{III}(NH_3)_4(Cat\text{-}CO_2H)]^+$ are *ca.* 6.3 and 4.6 respectively, while that for the carboxylic acid function of $[Ru^{II}(NH_3)_4(Q\text{-}CO_2H)]^{2+}$ is *ca.* 3.1. The −60 mV per pH unit dependence of the more negative wave below pH ≈ 3 is due to the dissociation to form $[Ru^{II}(NH_3)_4(H_2O)_2]^{2+}$.[62]

The species, R = H, show a similar pH dependence of the $[Ru^{III}(NH_3)_4(Cat\text{-}R)]^+/[Ru^{II}(NH_3)_4(Cat\text{-}R)]$ wave due to formation of $[Ru^{II}(NH_3)_4(H_2O)_2]^{2+}$ below about pH 3; however unlike the case with R = CO_2, this wave is pH independent above pH 3. The $[Ru^{II}(NH_3)_4(q\text{-}H)]^{2+}/[Ru^{III}(NH_3)_4(Cat\text{-}H)]^+$ wave is pH independent over the range 2–7. These data confirm that the pH dependence of the R = CO_2 species is localized at the CO_2 site.

FTIR

Studies of infrared spectra of the ligands in metal-transition complexes have provided useful information on the nature of the metal–ligand bond.[55] The effect of coordination may shift the frequency of a ligand vibration depending on its interaction with the metal. In ammine transition metal complexes the symmetric and asymmetric NH_3 stretches shift to lower energy

Table 8 Calculated (TD-DFRT) and experimental electronic spectral data for $[Ru(NH_3)_4(O_2C_6H_4)]^{2+/0}$ (in parentheses: electric dipole oscillator strengths, *f*), R = H series

Electronic transition (Principal excitation) $[Ru(NH_3)_4(Q)]^{2+}$ Ground state $^1A_1$			TD-DFRT(B3LYP) Excitation energy/eV (intensity)				Experiment
			LanL2DZ	SDD	CEP-121G	DZVP	
HOMO ⟶ LUMO	$d_{x^2-y^2}$ (Ru) ⟶ π*(Q)–d_{xz} (Ru)	$^1B_1$	0.65(0)	0.55(0)	0.66(0)	0.89(0)	
HOMO-1 ⟶ LUMO	d_{xy} (Ru)–π(Q) ⟶ π*(Q)–d_{xz} (Ru)	$^1B_2$	0.90(0)	0.81(0)	0.90(0)	1.11(0)	
HOMO-3 ⟶ LUMO	π(Q) + d_{xy} (Ru) ⟶ π*(Q)–d_{xz} (Ru)	$^1B_2$	2.08(0.0066)	2.06(0.0061)	2.08(0.0067)	2.21(0.0072)	[a]
HOMO-2 ⟶ LUMO	d_{yz} (Ru)–π(Q) ⟶ π*(Q)–d_{xz} (Ru)	$^1A_1$	2.48(0.22)	2.49(0.24)	2.42(0.23)	2.38(0.19)	2.41(0.065)
HOMO ⟶ LUMO+2	$d_{x^2-y^2}$ (Ru) ⟶ d_{yz} (Ru)	$^1B_2$	3.02(0.0002)	3.15(0.0002)[b]	2.92(0.0002)	2.76(0.0002)	2.75(sh)
HOMO ⟶ LUMO+1	$d_{z^2-y^2}$ (Ru) ⟶ d_{x^2} (Ru)	$^1A_1$	3.67(0.0002)	3.67(0)[b]	3.55(0)	3.44(0.0004)	3.45(sh)
HOMO-5 ⟶ LUMO	π(Q) ⟶ π*(Q)–d_{xz} (Ru)	$^1A_1$	4.34(0.027)	4.34(0.018)	4.35(0.031)	4.54(0.042)	4.56(intense)
$[Ru(NH_3)_4(Cat)]$ Ground state $^1A_1$							Experiment
HOMO ⟶ LUMO	d_{xz} (Ru) + π(Cat) ⟶ σ*(Ru,NH_3)	$^1B_1$	2.21(0.0014)	1.35(0.0022)	1.91(0.0034)	2.47(0.0028)	
HOMO-1 ⟶ LUMO	$d_{z^2-y^2}$ (Ru) ⟶ σ*(Ru,NH_3)	$^1A_1$	2.45(0.0019)	1.57(0.0027)	2.15(0.0041)	2.93(0.0068)	
HOMO ⟶ LUMO+3[c]	d_{xz} (Ru) + π(Cat) ⟶ π*(Cat)	$^1A_1$	4.04(0.047)	3.86(0.037)	4.06(0.039)	4.23(0.085)	4.69(intense)

INDO/S calculated data for the parent, R = H species, can be found as a footnote to Table 3. [a] Overlapping absorption bands. [b] Corresponds to HOMO ⟶ LUMO+3 and HOMO ⟶ LUMO+2 electron excitations in B3LYP/SDD calculations because of switched order of orbitals. [c] Corresponds to HOMO ⟶ LUMO+4 electron excitation with basis sets other than B3LYP/DZVP because of the switched order of orbitals.

in comparison to those of the "free" ligand while the degenerate deformation, symmetric deformation and rocking vibration of the coordinated ammonia shift to higher energy.[56–58] Band assignments for the various NH_3 modes occurring in the 600–4000 cm^{-1} region were made by comparison with the spectra of other ammine complexes of ruthenium and of the N-deuteriated derivatives (Table 1).

The N–H stretching frequencies of ruthenium ammine complexes may be used as a rough measure of Ru–N bond strength.[55,57] The rocking mode is the most sensitive to coordination and can be used to compare the M–N bond strength in a series of complexes.[55] The higher the energy of the rocking vibration the stronger is the M–NH_3 bond. The NH_3 rocking vibrational frequencies in $[Ru^{III}(NH_3)_4(Cat\text{-}R)]^+$ were compared with those in $[Ru^{III}(NH_3)_4(ox)]_2S_2O_6$[73] and $[Ru(NH_3)_6]Cl_n$ ($n = 2$ or 3)[55] (Table 1) and found at a substantially higher energy in these complexes than in either the oxalate complexes or the hexaammine, reflecting a significantly stronger interaction between ruthenium and the ammine group in the dioxolene complexes. This provides further evidence for the Ru^{III}–Cat rather than Ru^{II}–Sq formulation of the parent species.

Although infrared spectroscopy has proven to be a potent probe in determining the structure of transition-metal quinone complexes,[6,10,27,74–78] the FTIR data are not, curiously, fully supportive of the Ru^{III}–Cat formulation. Metal–catecholate complexes are often characterized by two intense bands at 1480 (ring stretch) and 1250 cm^{-1} (CO stretch) also found for the "free" ligand.[53,54] These bands gain intensity in transition metal catechol species due to coupling between the ring and CO stretching vibrations.[74] In the FTIR spectra of the $[Ru^{III}(NH_3)_4(Cat\text{-}R)]^+$ species (ESI Fig. S1; Table 1) diolato bands are observed at 1250 (medium intensity) and 1460 cm^{-1} (medium-weak intensity). Possibly, a strong interaction between the Ru^{III} and the CO bond has modified the ligand sufficiently that the strong band usually seen at 1480 cm^{-1} has substantially weakened and shifted to 1460 cm^{-1}.

Table 9 Energies, symmetries, and compositions of frontier orbitals of $[Ru(NH_3)_4(Cat)]$ calculated with B3LYP/DZVP

MO	Energy/eV	Symmetry	Ru (%)	NH_3 (%)	Cat (%)
LUMO+4	1.77	b_1	7	90	3
LUMO+3	1.50	b_1	0	2	98
LUMO+2	1.12	b_2	55	33	12
LUMO+1	0.96	a_1	72	23	5
LUMO	−0.15	a_1	85	25	−10
HOMO	**−3.35**	**b_1**	**23**	**2**	**75**
HOMO-1	**−4.00**	**a_1**	**87**	**3**	**11**
HOMO-2	**−4.00**	**a_2**	**67**	**3**	**29**
HOMO-3	**−4.51**	**b_1**	**69**	**3**	**28**
HOMO-4	**−4.98**	**a_2**	**23**	**1**	**76**
HOMO-5	−6.15	a_1	14	2	85

Electronic structure (Tables 9–11)

Tables 9–11 show the populations of frontier orbitals in terms of % contributions from atomic orbitals of the central atom and the ligands, using the Mulliken population analysis from the B3LYP/DZVP calculations. Some of the gross orbital populations are negative, which is a frequent problem of the Mulliken population analysis.[50b] Since the DZVP basis set is the largest among those we used, and provides excellent agreement with the experimental electronic spectrum, we use this to describe the molecular orbitals of the various complexes.

The "free" ligand LUMO has b_1 symmetry while the HOMO has a_2 symmetry. The frontier $d(t_{2g})$ orbitals transform as b_1 (d_{xz}, π symmetry), a_2 (d_{xz}, δ symmetry) and a_1 (d_{z^2}, σ symmetry) where the symmetry noted is with respect to the dioxolene ligand. We discuss specifically interactions within this group of five orbitals (bold in Tables 9–11). It is the bonding and antibonding interactions between these b_1 and a_2 ligand orbitals and the b_1 and a_2 d orbitals, respectively, which are primarily responsible for the mixing between metal and ligand.

In the quinone oxidation state ($[Ru^{II}(NH_3)_4(Q)]^{2+}$) the LUMO is predominantly a quinone π* orbital of b_1 symmetry and is the antibonding combination of the "free" ligand b_1 π* LUMO and d_{xz}. This orbital is progressively filled as the species is reduced and becomes the HOMO in the doubly reduced $[Ru^{II}(NH_3)_4(Cat)]$. The three $d(t_{2g})$ orbitals lying below this b_1 orbital are a_1, a_2 and b_1, in this sequence, being the same for all three oxidation states, *i.e.* with the b_1 orbital being the most stable. The a_1 and a_2 orbitals generally lie very close together, while the b_1 is stabilized due to being comprised of the bonding combination of d_{xz} with the ligand π* b_1 orbital. The $d(t_{2g})$ splitting energies are very similar, in the range from 0.35 to 0.7 eV for all three oxidation states. Clearly, the lower energy b_1 is mainly metal in character while the higher energy b_1 is mainly localized on the ligand. This mostly ligand b_1 orbital however has approximately 20% ruthenium character in all three oxidation states in the DFT calculation.

Just below this set of t_{2g} orbitals is a filled ligand π orbital of a_2 symmetry which was the HOMO in the "free" ligand. The pair of a_2 orbitals are formed from the bonding and antibonding interactions between metal d_{xy} and "free" ligand π-a_2 HOMO. In this case the lower a_2 orbital is mostly localized on the ligand but consists of approximately 20% d_{xy} in all three oxidation states. This 20% mixing of Ru into the ligand orbital, true also for the b_1 orbital, is a common observation in dioxolene ruthenium complexes.[13,34c,f]

The calculations illustrate that, aside from electron occupancy, there is not much difference in electronic structure between the formal $[Ru^{II}(NH_3)_4(Q)]^{2+}$ and supposed $[Ru^{III}(NH_3)_4(Cat)]^+$ species. This would reinforce the view that the latter species contains a significant contribution from $[Ru^{II}(NH_3)_4(Sq)]^+$.

Table 10 Energies, symmetries, and compositions of frontier orbitals of $[Ru(NH_3)_4(Cat)]^+$ calculated with B3LYP/DZVP

MO	Energy/eV	Symmetry	Ru (%)	NH_3 (%)	Cat (%)
LUMO+4	−2.89 (−2.58)	b_1	0 (0)	1 (1)	99 (99)
LUMO+3	−3.32 (−3.24)	b_2	74 (74)	13 (13)	13 (14)
LUMO+2	−3.48 (−3.42)	a_1	74 (74)	21 (21)	5 (5)
LUMO+1	−3.70 (−3.69)	a_1	78 (77)	33 (33)	−10 (−10)
SOMO	**−8.11 (−6.22)**	**b_1**	**22 (16)**	**1 (1)**	**77 (83)**
HOMO-1[a]	**−8.63 (−8.54)**	**a_1**	**85 (84)**	**3 (3)**	**12 (13)**
HOMO-2[a]	**−8.68 (−8.49)**	**a_2**	**73 (62)**	**3 (3)**	**24 (35)**
HOMO-3	**−9.31 (−8.71)**	**b_1**	**70 (75)**	**3 (3)**	**27 (23)**
HOMO-4	**−9.56 (−9.39)**	**a_2**	**19 (29)**	**1 (1)**	**80 (70)**
HOMO-5	−10.91 (−10.79)	a_1	13 (14)	2 (2)	85 (84)

Data for beta-spin orbitals are given in parentheses. [a] HOMO-1(α) corresponds to HOMO-2(β), HOMO-2(α) to HOMO-1(β).

Table 11 Energies, symmetries, and compositions of frontier orbitals of $[Ru(NH_3)_4(Q)]^{2+}$ calculated with B3LYP/DZVP

MO	Energy/eV	Symmetry	Ru (%)	NH_3 (%)	Cat (%)
LUMO+4	−7.17	a_2	1	0	99
LUMO+3	−7.21	a_1	73	37	−10
LUMO+2	−7.99	b_2	75	14	11
LUMO+1	−8.02	a_1	72	24	4
LUMO	**−11.13**	**b_1**	**16**	**1**	**83**
HOMO	**−13.25**	**a_1**	**84**	**3**	**14**
HOMO-1	**−13.32**	**a_2**	**73**	**3**	**24**
HOMO-2	**−13.60**	**b_1**	**76**	**3**	**22**
HOMO-3	**−14.15**	**a_2**	**20**	**1**	**79**
HOMO-4	−15.63	a_1	13	3	85
HOMO-5	−16.22	b_1	4	7	90

Nature of the bonding

The IR data suggest that the parent complex is well described as Ru^{III}–Cat whereas the EPR data do not show clear ruthenium(III) signals (3 *g* values) under any conditions although the absence of room temperature signals is evidence for Ru^{III} rather than an organic free radical. The calculations show significant covalency between the metal and ligand but with the closest localized description, for the gas phase calculation of the parent species, being Ru^{II}–Sq. A preliminary calculation using a dielectric continuum to model the solvent does however show that the presence of solvent causes an increase in the spin density on the ruthenium atom of some 60–95%, depending on basis set, reaching 0.52 with the B3LYP/LanL2DZ calculation, *i.e.* the calculation predicts that solvent makes the species more Ru^{III}-like, consistent with the EPR data in neutral solution. It is probable that the real electronic distribution lies between Ru^{II} and Ru^{III} with the b_1 mixed orbitals being closer to 50 ± 10% Ru + 50 ± 10% dioxolene.

With similar extensive covalency involving the frontier a_2 orbitals, the changes in electronic spectra observed, for the parent species, with change of temperature and/or medium may reflect small variations in the extent of mixing caused by solvent–solute interactions. In such highly mixed species we expect relatively little solvatochromism since the ground and excited state of the visible region principal absorption band will have very similar geometry and dipole moment. This is in contrast to species such as $[Ru(NH_3)_5(py)]^{2+}$ where the extent of mixing is much smaller, the MLCT state will possess a rather different dipole moment from the ground state, and the system will be much more solvatochromic.[79–81] In this case gas phase calculations using INDO/S or TD-DFRT do not reproduce the solution spectra well. For example, while experiment shows the principal visible region MLCT band at 24600 cm^{-1} ($f = 0.16$),[82] calculations yield 35900,[83] 34500 cm^{-1} ($f = 0.39$),[82] or, using TD-DFRT (B3LYP/DZVP), we find 32900 cm^{-1} ($f = 0.11$). When solvent (water) is incorporated into the calculation there is a red shift to 30600[82] or 27700 cm^{-1}[83] approaching the experimental value.[82,83]

With this magnitude of mixing the effect on the electronic spectrum of protonation of the $R = CO_2^-$ group might well be very small. The effect of acid seems to be identical for the $R = CO_2^-$ substituted complex, as for the unsubstituted, R = H, complex (Table 4) leading us to conclude that we may be seeing a solvent effect and that protonation of CO_2^- does not significantly affect the electronic structure.

Electronic spectra (Tables 3, 8)

The predicted spectra using TD-DFRT are shown in Table 8.

$[Ru^{II}(NH_3)_4(Q\text{-}R)]^{2+}$ [Ground state $^1A_1$]. The visible spectra of the quinone complexes showing a strong charge transfer (CT) band near 19400 cm^{-1} (2.4 eV) are typical of ruthenium(II) complexes of this oxidation state.[12,13,17,24,26] These bands are fairly narrow, indicative of substantial mixing between the Ru^{II}–Q ground state and Ru^{III}–Sq excited state. The bandwidth is similar to that (1740 cm^{-1}) observed for the comparable band in the similarly mixed $[Ru(NH_3)_4(bqdi)]^{2+}$ (bqdi = *o*-benzoquinone diimine).[13]

According to TD-DFRT calculations the intense visible region absorption is assigned to a $d_{xz}(Ru) + \pi^*(Q) \longrightarrow \pi^*(Q) \longrightarrow d_{xz}(Ru)$ transition, *i.e.* HOMO-2 (b_1) ⟶ LUMO (b_1) MLCT. Of the various functionals investigated the B3LYP/DZVP gives the best agreement with the experimental data (Table 8, R = H); indeed the agreement is excellent.

Electronic transitions originating from the other two $d(t_{2g})$ orbitals, HOMO (a_1) and HOMO-1 (a_2), to LUMO have not been observed experimentally. The TD-DFRT calculations show that these transitions should occur in the near IR region, but their intensity should be very low (see Table 8). There is another transition, HOMO-3 (a_2) (mixed with HOMO-1, a_2) ⟶ LUMO, which has energy comparable to, but intensity lower than that of the HOMO-2 ⟶ LUMO major band. This does not appear as a separate band in the experimental spectra but may be responsible for the low energy tail on the 19200 cm^{-1} band (see Fig. 3). The two weaker features seen as shoulders in the experimental spectrum are d–d transitions according to the TD-DFRT calculations.

The UV region band is the expected internal $\pi \longrightarrow \pi^*$ quinone ligand transition, formally, according to TD-DFRT calculations, from HOMO-5 to LUMO.

$[Ru^{III}(NH_3)_4(Cat\text{-}R)]^+$ [Ground state $^2B_1$]. These parent species show a single broad band in the visible region of lower intensity than the visible region band of the Q-R complexes. Ruthenium bipyridine complexes containing the Ru^{II}–Sq fragment display a strong and narrow band in the near infrared region. The broad band seen for these parent complexes near 14000–15000 cm^{-1} is at substantially higher energy and much broader perhaps because of a greater contribution from $[Ru^{III}(Cat)]$. This broad band is assigned to the same transition as in the quinone oxidation state, *i.e.* $b_1 \longrightarrow b_1$. TD-DFRT code to predict the electronic spectra of open shell species is not yet generally available. We therefore carried out a restricted open shell INDO/S calculation on the DFT B3LYP/DZVP geometry. This predicted the main visible region band at 14000 cm^{-1} (R = H) in excellent agreement with experiment and confirmed its assignment as $b_1 \longrightarrow b_1$ (HOMO-3 ⟶ SOMO) (Tables 3, 10).

In the case of $R = CO_2^-$ there is an extra strong UV transition generated through coupling between the ligand π^* and CO_2 function. The inverse shift in energy with variation of R to the band in the Ru^{II}(Q-R) species would be consistent with the direction of charge displacement being reversed in this species relative to the quinone species,[81,84–86] *i.e.* that the main band of the $[Ru(NH_3)_4(Q\text{-}R)]^{(n+1)+}$ species is MLCT while the broad band of these parent ruthenium(III) species has LMCT character. LMCT character is also supported by the blue rather than red shift when the $R = CO_2^-$ species is protonated.

Although a very limited data set, it was reasonable to question whether these data correlate with Hammett substituent constants.[87] Indeed there is an approximately linear relationship, for both oxidation states, with the field/inductive parameter σ_m. However the slope of this relationship is the inverse of that expected with the MLCT band shifting to the red as the substituent becomes more negative. Since these transitions (see below) involved the π framework of the molecule, the inductive effect may not be relevant here. Indeed there is also a linear correlation with the Resonance parameter,[87] and this does possess a slope consistent with the expectation that a π-mesomeric effect moving charge into the ligand will shift the MLCT band to the blue and the LMCT band to the red.

However the data spread is rather too small to draw a firm conclusion. Variations in the Coulomb (J) and exchange (K) integrals[88] with R could cause a CT band to shift in the inverse sense to that predicted upon a simple consideration of MLCT or LMCT. Nevertheless the optical experimental data do seem best understood in terms of a $[Ru^{III}(NH_3)_4(Cat\text{-}R)]^{n+}$ description for the parent species.

Given the valence tautomerism observed in many other dioxolene species[1b–e,h,i,k,l,6,10,27–31,34–36] the temperature dependence of the spectra of the $[Ru^{III}(NH_3)_4(Cat\text{-}R)]^+$ species was explored. Indeed the visible region LMCT band shows significant thermochromism (Table 4, Fig. 4). In a MeOH–EtOH–water mixture the visible region LMCT band shifts up to 1500 cm^{-1} to the blue, from room to liquid nitrogen temperature. In 0.1 M HCl–MeOH–EtOH the effect is even more marked (1700 cm^{-1} blue shift). However the band does not sharpen, but remains very broad. The EPR evidence presented above shows that at low temperature, in this medium, the species is more closely represented by the description $[Ru^{II}(NH_3)_4(Sq)]^+$.

$[Ru^{II}(NH_3)_4(Cat\text{-}R)]$ [Ground state $^1A_1$]. These species show strong absorption only in the UV region caused by $\pi \longrightarrow \pi^*$ transitions of the catechol ligand. According to TD-DFRT calculations the strongest electronic transition is from HOMO to LUMO+3. The calculations predict two low-intensity electronic transitions in the visible region, but we suppose that this may be an artifact of the calculation on the isolated molecule. These transitions are the electron transfer from HOMO ($d_{xz} - \pi$) and HOMO-1 ($d_{z^2-y^2}$) to the LUMO which is the σ^* orbital localized on Ru and the NH_3 ligands. It has been noticed[51c] that the TD-DFRT method works well only if the excitation energies do not exceed the negative of the HOMO energy, $-\varepsilon_{HOMO}$, where the ionization continuum begins, and if transitions to unbound virtual orbitals are not involved. The HOMO and LUMO energies of $[Ru(NH_3)_4(Cat)]$ are quite high (around −3 eV and 0 respectively) and, in this situation, it is to be expected that the TD-DFRT excitation energies will be very sensitive to the diffuseness of the basis set. Since solvation of $[Ru(NH_3)_4(Cat)]$ by water molecules affects the energies of the orbitals, calculation of the excitation energies would possibly be more accurate if the TD-DFRT/SCRF code were available.

It is of interest that for $R = CO_2$ there are two $\pi \longrightarrow \pi^*$ transitions between 30000 and 40000 cm^{-1} for this Ru^{II}–Cat-CO_2 species. There are also two such transitions for the Ru^{III}–Cat-CO_2 species but only one for the Ru^{II}–Q-CO_2 species. Thus there is yet additional evidence for the validity of the Ru^{III}–Cat-R formulation of the parent species.

Conclusion

Attempts to describe these species in terms of a single oxidation state are probably not useful. This is especially true of the parent species which, under various conditions, displays properties of both $[Ru^{III}(NH_3)_4(Cat)]^+$ and $[Ru^{II}(NH_3)_4(Sq)]^+$. We do not appear to be observing valence tautomerism in the sense that one species exists at low temperature, or under specified conditions, and is converted into the other above a certain temperature. Rather there is very substantial covalency between metal and ligand orbitals such that these species behave rather like delocalized organic molecules. In solution a change of temperature changes the solvent characteristics and, through solvent interactions, the extent of delocalization is modified causing the small spectroscopic shifts. The evidence for this lies in the electronic structural calculations and spectroscopic assignments. An abrupt change from MLCT behavior in $[Ru^{II}(NH_3)_4(Q)]^{2+}$ species to LMCT behavior in $[Ru^{III}(NH_3)_4(Cat)]^+$ is not observed. Rather, both these species have remarkably similar electronic structures in terms of mixing of the frontier orbitals and differ only in the electron occupancy of these orbitals. Interestingly, the major spectroscopic features have the same provenance in both the parent and oxidized species. DFT B3LYP/DZVP provides a very adequate description of these species, and TD-DFRT is effective in predicting the electronic spectra of the closed shell species very accurately. Although such calculations are "gas phase" and we are comparing with experimental data in solution, this may be reasonable due to the small solvatochromism anticipated for these highly mixed species.

Acknowledgements

We thank the Natural Sciences and Engineering Research Council (Ottawa), CNPq, CAPES, PADCT and FAPESP (Brazil) for financial support.

References

1 (*a*) S. R. Sofen, D. C. Ware, S. R. Cooper and K. N. Raymond, *Inorg. Chem.*, 1979, **18**, 234; (*b*) N. C. Fletcher, T. C. Robinson, A. Behrendt, J. C. Jeffery, Z. R. Reeves and M. D. Ward, *J. Chem. Soc., Dalton Trans.*, 1999, 2999; (*c*) E. A. Robinson and J. E. Earley, *Inorg. Chem.*, 1999, **38**, 4128; (*d*) R. M. Ramadan, M. S. A Hamza, A. E.-N. M. Salem and F. M. El-Zawawy, *Transition Met. Chem.*, 1999, **24**, 193; (*e*) A. D. Shukla, B. Whittle, H. C. Bajaj, A. Das and M. D. Ward, *Inorg. Chim. Acta*, 1999, **285**, 89; (*f*) M. Ebadi and A. B. P. Lever, *Inorg. Chem.*, 1999, **38**, 467; (*g*) A. M Barthram, R. L. Cleary, R. Kowallick and M. D. Ward, *Chem. Commun.*, 1998, 2695; (*h*) T. E. Keyes, R. J. Forster, P. M. Jayaweera, C. G. Coates, J. J. McGarvey and J. G. Vos, *Inorg. Chem.*, 1998, **37**, 5925; (*i*) K. N. Mitra, S. Choudhury, A. Castineiras and S. Goswami, *J. Chem. Soc., Dalton Trans.*, 1998, 2901; (*j*) K. N. Mitra, S. Goswami and S.-M. Peng, *Chem. Commun.*, 1998, 1685; (*k*) G. D. Storrier, S. B. Colbran and D. C Craig, *J. Chem. Soc., Dalton Trans.*, 1998, 1351; (*l*) A. M. Barthram, R. L. Cleary, J. C. Jeffery, S. M. Couchman and M. D. Ward, *Inorg. Chim. Acta*, 1998, **267**, 1; (*m*) P. L. Hill, L. Y. Lee, T. R. Younkin, S. D. Orth and L. McElwee-White, *Inorg. Chem.*, 1997, **36**, 5655.
2 S. L. Kessel, R. M. Emberson, P. G. Debrunner and D. N. Hendrickson, *Inorg. Chem.*, 1980, **19**, 1170.
3 C. G. Pierpont and R. M. Buchanan, *Coord. Chem. Rev.*, 1981, **38**, 45.
4 M. W. Lynch, D. N. Hendrickson, B. R. Fitzgerald and C. G. Pierpont, *J. Am. Chem. Soc.*, 1981, **103**, 3961.
5 M. D. Stallings, M. M. Morrison and D. T. Sawyer, *Inorg. Chem.*, 1981, **20**, 2655.
6 M. W. Lynch, M. Valentine and D. N. Hendrickson, *J. Am. Chem. Soc.*, 1982, **104**, 6982.
7 R. M. Buchanan, J. Claflin and C. G. Pierpont, *Inorg. Chem.*, 1983, **22**, 2552.
8 M. E. Bodini, G. Copia, R. Robinson and D. T. Sawyer, *Inorg. Chem.*, 1983, **22**, 126.
9 M. I. Kabachnik, N. N. Bubnov, S. P. Solodnikov and A. I. Prokofev, *Russ. Chem. Rev.* (*Engl. Transl.*), 1984, **5**, 37.
10 M. W. Lynch, D. N. Hendrickson, B. J. Fitzgerald and C. G. Pierpont, *J. Am. Chem. Soc.*, 1984, **106**, 2041.
11 M. E. Cass, N. R. Gordon and C. G. Pierpont, *Inorg. Chem.*, 1986, **25**, 3962.
12 M. A. Haga, E. S. Dodsworth, A. B. P. Lever, R. S. Boone and C. G. Pierpont, *J. Am. Chem. Soc.*, 1986, **108**, 7413; M. A. Haga, E. S. Dodsworth and A. B. P. Lever, *Inorg. Chem.*, 1986, **25**, 447.
13 R. A. Metcalfe and A. B. P. Lever, *Inorg. Chem.*, 1997, **36**, 4762.
14 J. R. Bradbury and F. A. Schultz, *Inorg. Chem.*, 1986, **25**, 4416.
15 C. Bianchini, D. Masi, C. Mealli, G. Martini, F. Laschi and P. Zanello, *Inorg. Chem.*, 1987, **26**, 3683.
16 W. Kaim, *Coord. Chem. Rev.*, 1987, **76**, 187.
17 A. B. P. Lever, P. R. Auburn, E. S. Dodsworth, M. Haga, W. Liu, M. Melnik and A. Nevin, *J. Am. Chem. Soc.*, 1988, **110**, 8076.
18 D. J. Stufkens, T. L. Snoeck and A. B. P. Lever, *Inorg. Chem.*, 1988, **27**, 953.
19 C. P. Cheng, S. R. Wang, J. C. Lin and S. L. Wang, *J. Organomet. Chem.*, 1988, **249**, 375.
20 C. Benelli, A. Dei, D. Gatteschi and L. Pardi, *Inorg. Chem.*, 1989, **163**, 99.
21 E. S. Dodsworth and A. B. P. Lever, *Chem. Phys. Lett.*, 1990, **172**, 151.
22 F. Hartl, A. Vlcek, Jr., L. A. deLarie and C. G. Pierpont, *Inorg. Chem.*, 1990, **29**, 1073.
23 S. Bhattacharya and C. G. Pierpont, *Inorg. Chem.*, 1991, **30**, 1511.

24 P. R. Auburn, E. S. Dodsworth, M. Haga, W. Liu, W. A. Nevin and A. B. P. Lever, *Inorg. Chem.*, 1991, **30**, 3502.
25 F. Hartl and A. Vlcek, Jr., *Inorg. Chem.*, 1991, **30**, 2402.
26 (*a*) H. Masui, A. B. P. Lever and P. R. Auburn, *Inorg. Chem.*, 1991, **30**, 2402; (*b*) H. Masui, A. B. P. Lever and E. S. Dodsworth, *Inorg. Chem.*, 1993, **32**, 258.
27 A. Caneschi and A. Dei, *Angew. Chem., Int. Ed.*, 1998, **37**, 3005; D. Ruiz, J. Yoo, D. N. Hendrickson, I. A. Guzei and A. L. Rheingold, *Chem. Commun.*, 1998, 208; S. A. Attia and C. G. Pierpont, *Inorg. Chem.*, 1998, **37**, 3051; S. A. Attia and C. G. Pierpont, *Inorg. Chem.*, 1997, **36**, 6184; D. M. Adams, L. Noodleman and D. N. Hendrickson, *Inorg. Chem.*, 1997, **36**, 3966; D. M. Adams and D. N. Hendrickson, *J. Am. Chem. Soc.*, 1996, **118**, 11515; C. Roux, D. M. Adams, J. P. Itie, A. Polian, D. N. Hendrickson and M. Verdaguer, *Inorg. Chem.*, 1996, **35**, 2846; D. M. Adams, B. Li, J. D. Simon and D. N. Hendrickson, *Angew. Chem., Int. Ed. Engl.*, 1995, **34**, 1481; C. G. Pierpont and O.-S. Jung, *Inorg. Chem.*, 1995, **34**, 4281; S. A. Attia and C. G. Pierpont, *Inorg. Chem.*, 1995, **34**, 1172; S. A. Attia, O.-S. Jung and C. G. Pierpont, *Inorg. Chim. Acta*, 1994, **226**, 91; D. M. Adams, A. Dei, A. L. Rheingold and D. N. Hendrickson, *J. Am. Chem. Soc.*, 1993, **115**, 8221; D. M. Adams, A. Dei, A. L. Rheingold and D. N. Hendrickson, *Angew. Chem.*, 1993, **105**, 954; M. Kurihara, S. Daniele, K. Tsuge, H. Sugimoto and K. Tanaka, *Bull. Chem. Soc. Jpn.*, 1998, **71**, 867.
28 J. S. Thompson and J. C. Calabrese, *Inorg. Chem.*, 1985, **24**, 3167.
29 C. G. Pierpont, S. K. Larsen and S. R. Boone, *Pure Appl. Chem.*, 1988, **60**, 1331.
30 D. M. Adams, A. Dei, A. L. Rheingold and D. N. Hendrickson, *Angew. Chem., Int. Ed. Engl.*, 1993, **32**, 880.
31 A. Dei, *Inorg. Chem.*, 1993, **32**, 5730.
32 A. B. P. Lever, H. Masui, R. A. Metcalfe, D. J. Stufkens, E. S. Dodsworth and P. R. Auburn, *Coord. Chem. Rev.*, 1993, **125**, 317.
33 P. R. Auburn and A. B. P. Lever, *Inorg. Chem.*, 1990, **29**, 2551; R. A. Metcalfe, E. S. Dodsworth, S. S. Fielder, D. J. Stufkens, A. B. P. Lever and W. J. Pietro, *Inorg. Chem.*, 1996, **35**, 7741; R. A. Metcalfe, L. C. G. Vasconcellos, H. Mirza, D. W. Franco and A. B. P. Lever, *J. Chem. Soc., Dalton Trans.*, 1999, 2653; C. J. da Cunha, S. S. Fielder, D. V. Stynes, H. Masui, P. R. Auburn and A. B. P. Lever, *Inorg. Chim. Acta*, 1996, **249**, 293; C. J. da Cunha, E. S. Dodsworth, M. A. Monteiro and A. B. P. Lever, *Inorg. Chem.*, 1999, **38**, 5399; H. Masui, A. L. Freda, M. C. Zerner and A. B. P. Lever, *Inorg. Chem.*, 2000, **39**, 141.
34 A. L. Jorgenson, R. A. Nadeau, V. G. Young, Jr. and W. L. Gladfelter, *J. Organomet. Chem.*, 1998, **563**, 1.
35 M. Kondo, M. Hamatani, S. Kitagawa, C. G. Pierpont and K. Unoura, *J. Am. Chem. Soc.*, 1998, **120**, 455; M. Kurihara, S. Daniele, K. Tsuge, H. Sugimoto and K. Tanaka, *Bull. Chem. Soc. Jpn.*, 1998, **71**, 867C.
36 G. D. Storrier, K. Takada and H. D. Abruna, *Inorg. Chem.*, 1999, **38**, 559.
37 D. N. Beratan, J. N. Onuchic and J. J. Hopfield, in *Molecular Electronics – Biosensors, Biocomputers*, ed. F. T. Hong, Plenum Press, New York, 1989, p. 353.
38 S. D. Pell, R. B. Salmonsen, A. Abelleira and M. J. Clarke, *Inorg. Chem.*, 1984, **23**, 385.
39 T. Matsubara and P. C. Ford, *Inorg. Chem.*, 1976, **15**, 1107.
40 A. D. Allen and F. Bottomley, *Can. J. Chem.*, 1968, **46**, 469.
41 R. S. Silva, E. Tfouni and A. B. P. Lever, *Inorg. Chim. Acta*, 1995, **235**, 427.
42 (*a*) M. C. Zerner, ZINDO program, version 98.1, Quantum Theory Project, University of Florida, Gainesville, FL, 1998; (*b*) J. Zeng, N. S. Hush and J. R. Reimers, *J. Am. Chem. Soc.*, 1996, **118**, 2059; (*c*) J. Zeng, N. S. Hush and J. R. Reimers, *J. Phys. Chem.*, 1996, **100**, 19292; (*d*) J. Zeng, N. S. Hush and J. R. Reimers, *J. Phys. Chem.*, 1995, **99**, 10459.
43 GAUSSIAN 98, Revision A.7, M. J. Frisch, G. W. Trucks, H. B. Schlegel, G. E. Scuseria, M. A. Robb, J. R. Cheeseman, V. G. Zakrzewski, J. A. Montgomery, Jr., R. E. Stratmann, J. C. Burant, S. Dapprich, J. M. Millam, A. D. Daniels, K. N. Kudin, M. C. Strain, O. Farkas, J. Tomasi, V. Barone, M. Cossi, R. Cammi, B. Mennucci, C. Pomelli, C. Adamo, S. Clifford, J. Ochterski, G. A. Petersson, P. Y. Ayala, Q. Cui, K. Morokuma, D. K. Malick, A. D. Rabuck, K. Raghavachari, J. B. Foresman, J. Cioslowski, J. V. Ortiz, B. B. Stefanov, G. Liu, A. Liashenko, P. Piskorz, I. Komaromi, R. Gomperts, R. L. Martin, D. J. Fox, T. Keith, M. A. Al-Laham, C. Y. Peng, A. Nanayakkara, C. Gonzalez, M. Challacombe, P. M. W. Gill, B. Johnson, W. Chen, M. W. Wong, J. L. Andres, C. Gonzalez, M. Head-Gordon, E. S. Replogle and J. A. Pople, Gaussian, Inc., Pittsburgh, PA, 1998.
44 A. D. Becke, *J. Chem. Phys.*, 1993, **98**, 5648.
45 C. Lee, W. Yang and R. G. Parr, *Phys. Rev. B*, 1988, **37**, 785.
46 W. J. Stevens, H. Basch and J. Krauss, *J. Chem. Phys.*, 1984, **81**, 6026; W. J. Stevens, M. Krauss, H. Basch and P. G. Jasien, *Can. J. Chem.*, 1992, **70**, 612; T. R. Cundari and W. J. Stevens, *J. Chem. Phys.*, 1993, **98**, 5555.
47 T. H. Dunning, Jr. and P. J. Hay, in *Methods of Electronic Structure, Theory*, ed. H. F. Schaefer III, Plenum Press, 1977, vol. 2; P. J. Hay and W. R. Wadt, *J. Chem. Phys.*, 1985, **82**, 270; P. J. Hay and W. R. Wadt, *J. Chem. Phys.*, 1985, **82**, 284; P. J. Hay and W. R. Wadt, *J. Chem. Phys.*, 1985, **82**, 299.
48 P. Fuentealba, H. Preuss, H. Stoll and L. v. Szentpaly, *Chem. Phys. Lett.*, 1989, **89**, 418; L. v. Szentpaly, P. Fuentealba, H. Preuss and H. Stoll, *Chem. Phys. Lett.*, 1982, **93**, 555; P. Fuentealba, H. Stoll, L. v. Szentpaly, P. Schwerdtfeger and H. Preuss, *J. Phys. B*, 1983, **16**, 1323; H. Stoll, P. Fuentealba, P. Schwerdtfeger, J. Flad, L. v. Szentpaly and H. Preuss, *J. Chem. Phys.*, 1984, **81**, 2732; P. Fuentealba, L. v. Szentpaly, H. Preuss and H. Stoll, *J. Phys. B*, 1985, **18**, 1287.
49 N. Godbout, D. R. Salahub, J. Andzelm and E. Wimmer, *Can. J. Chem.*, 1992, **70**, 560; basis sets were obtained from the Extensible Computational Chemistry Environment Basis Set Database, Version 1.0, as developed and distributed by the Molecular Science Computing Facility, Environmental and Molecular Sciences Laboratory which is part of the Pacific Northwest Laboratory, Richland, Washington, and funded by the U.S. Department of Energy. The Pacific Northwest Laboratory is a multi-program laboratory operated by Battelle Memorial Institute for the U.S. Department of Energy under contract DE-AC06-76RLO 1830. Contact David Feller or Karen Schuchardt for further information.
50 (*a*) MOMIX Program, Revision 4.3, S. I. Gorelsky and A. B. P. Lever, York University, Canada, 2000, available at http://www.chem.yorku.ca/grad/SG/; (*b*) S. M. Bachrach, in *Reviews in Computational Chemistry*, eds. K. B. Lipkowitz and D. B. Boyd, VCH Publishers Inc., New York, 1994, vol. 5, p. 177.
51 (*a*) M. E. Casida, in *Recent Advances in Density Functional Methods*, ed. D. P. Chong, World Scientific, Singapore, 1995, part 1, pp. 155–192; (*b*) M. E. Casida, in *Recent Developments and Applications of Modern Density Functional Theory, Theoretical and Computational Chemistry*, ed. J. M. Seminario, Elsevier, Amsterdam, 1996, vol. 4; (*c*) M. E. Casida, C. Jamorski, K. C. Casida and D. R. Salahub, *J. Chem. Phys.*, 1998, **108**, 4439; (*d*) R. E. Stratmann, G. E. Scuseria and M. J. Frisch, *J. Chem. Phys.*, 1998, **109**, 8218.
52 M. W. Wong, M. J. Frisch and K. B. Wiberg, *J. Am. Chem. Soc.*, 1991, **113**, 4776; M. W. Wong, K. B. Wiberg and M. J. Frisch, *J. Am. Chem. Soc.*, 1992, **114**, 523; M. W. Wong, K. B. Wiberg and M. J. Frisch, *J. Chem. Phys.*, 1991, **95**, 8991; M. W. Wong, K. B. Wiberg and M. J. Frisch, *J. Am. Chem. Soc.*, 1992, **114**, 1645; J. G. Kirkwood, *J. Chem. Phys.*, 1934, **2**, 351.
53 Y. Murakami, K. Nakamura and M. Tokunaga, *Bull. Chem. Soc. Jpn.*, 1963, **36**, 669.
54 H. A. Szymanski, *Interpreted Infrared Spectra*, Plenum Press, New York, 1967, vol. 3, p. 23; H. W. Wilson, *Spectrochim. Acta*, *Part A*, 1974, **30**, 2141.
55 K. Nakamoto, *Infrared and Raman Spectra of Inorganic and Coordination Compounds*, John Wiley, New York, 4th edn., 1986, p. 191, and references therein.
56 J. Fujita, K. Nakamoto and M. Kobayashi, *J. Chem. Soc.*, 1956, 3295.
57 T. Shimanouchi and I. Nakagawa, *Inorg. Chem.*, 1964, **3**, 1805.
58 W. P. Griffith, *J. Chem. Soc. A*, 1966, 899.
59 A. D. Allen, F. Bottomley, R. O. Harris, V. P. Reinsalu and C. V. Senoff, *J. Am. Chem. Soc.*, 1967, **89**, 5595.
60 P. H. Rieger, *Coord. Chem. Rev.*, 1994, **135/136**, 203, and references therein; A. R. Chakravarty and A. Chakravorty, *Inorg. Chem.*, 1981, **20**, 3138; N. Bag, G. K. Lahiri and A. Chakravorty, *J. Chem. Soc., Dalton Trans.*, 1990, 1557; G. K. Lahiri, S. Bhattacharya, M. Mukherjee, A. K. Mukherjee and A. Chakravorty, *Inorg. Chem.*, 1987, **26**, 3359; G. K. Lahiri, S. Bhattacharya, B. K. Ghosh and A. Chakravorty, *Inorg. Chem.*, 1987, **26**, 4324; H. K. Gupta and S. Dikshit, *Polyhedron*, 1987, **6**, 1009; N. S. Hush and A. Edgar, *Chem. Phys. Lett.*, 1980, **69**, 128; K. Matsumoto, T. Matsumoto, M. Kawano, H. Ohnuki, Y. Shichi, T. Nishide and T. Sato, *J. Am. Chem. Soc.*, 1996, **118**, 3597.
61 R. S. Nicholson and I. Shain, *Anal. Chem.*, 1964, **36**, 706.
62 A. J. Cohen and N. C. Handy, *Chem. Phys. Lett.*, 2000, **316**, 160.
63 M. E. Gress, C. Creutz and C. O. Quicksall, *Inorg. Chem.*, 1981, **20**, 1522; I. M. Treitel, M. T. Flood, R. E. Marsh and H. B. Gray, *J. Am. Chem. Soc.*, 1969, **91**, 6512; H. C. Stynes and J. A. Ibers,

Inorg. Chem., 1971, **10**, 2304; F. C. March and G. Ferguson, *Can. J. Chem.*, 1971, **49**, 3590; F. Bottomley, *J. Chem Soc.*, *Dalton Trans.*, 1972, 2148; J. K. Beatty, N. S. Hush, P. R. Taylor, C. L. Raston and A. H. White, *J. Chem. Soc.*, *Dalton Trans.*, 1977, 1121; D. E. Richardson, D. D. Walker, J. E. Sutton, K. O. Hodgson and H. Taube, *Inorg. Chem.*, 1979, **18**, 2216.
64 J. F. Wishart, A. Bino and H. Taube, *Inorg. Chem.*, 1986, **25**, 3318; T. W. Hambley and P. Lay, *Inorg. Chem.*, 1986, **25**, 4553; K. Krogh-Jespersen, J. D. Westbrook, J. A. Otienza and H. J. Schugar, *J. Am. Chem. Soc.*, 1987, **109**, 7025; R. J. Crutchley, K. McCaw, F. L. Lee and E. J. Gabe, *Inorg. Chem.*, 1990, **29**, 2576.
65 M. H. Chou, D. J. Szalda, C. Creutz and N. Sutin, *Inorg. Chem.*, 1994, **33**, 1674; F. Bottomley, *J. Chem. Soc.*, *Dalton Trans.*, 1974, 1600.
66 A. Broo, *Int. J. Quant. Chem. (Quant. Chem. Symp. 30)*, 1996, 1331.
67 O. Carugo, C. B. Castellani, K. Djinovic and M. Rizzi, *J. Chem. Soc.*, *Dalton Trans.*, 1992, 837.
68 S. I. Gorelsky, E. S. Dodsworth, A. B. P. Lever and A. A. Vlcek, *Coord. Chem. Rev.*, 1998, **174**, 469.
69 O. Ryba, J. Petranek and J. Pospisil, *Collect. Czech. Chem. Commun.*, 1965, **30**, 2157.
70 K. J. Vetter, *Electrochemical Kinetics*, Academic Press, New York, 1967, p. 483.
71 O. Ryba, J. Pilar and J. Petranek, *Collect. Czech. Chem. Commun.*, 1968, **33**, 26.
72 P. A. Christensen and A. Hamnett, *Techniques and Mechanisms in Electrochemistry*, Black Academic and Professional, New York, 1993, p. 27.
73 K. Gleu and W. Breuel, *Z. Anorg. Allg. Chem.*, 1938, **237**, 335.
74 D. J. Brown, C. G. Pierpont and J. T. Vogel, *Inorg. Nucl. Chem. Lett.*, 1976, **12**, 399.
75 R. M. Buchanan, S. L. Kessel, H. H. Downs, C. G. Pierpont and D. N. Hendrickson, *J. Am. Chem. Soc.*, 1978, **100**, 7894.
76 K. D. Magers, C. G. Smith and D. T. Sawyer, *Inorg. Chem.*, 1980, **19**, 492.
77 D. G. Brown and W. L. Johnson, *Z. Naturforsch.*, *Teil B*, 1979, **34**, 712.
78 W. P. Griffith, C. A. Pumphrey and T. A. Rainey, *J. Chem. Soc.*, *Dalton Trans.*, 1986, 1125.
79 Y. K. Shin, B. S. Brunschwig, C. Creutz and N. Sutin, *J. Phys. Chem.*, 1996, **100**, 8157.
80 J. Granifo, M. E. Vargas, E. S. Dodsworth, D. H. Farrar, S. S. Fielder and A. B. P. Lever, *J. Chem. Soc.*, *Dalton Trans.*, 1996, 4369.
81 A. B. P. Lever, *Inorganic Electronic Spectroscopy*, 2nd edn., Elsevier, New York, 1984, p. 205.
82 Y. K. Shin, D. J. Szalda, B. S. Brunschwig, C. Creutz and N. Sutin, *Inorg. Chem.*, 1997, **36**, 3190.
83 G. M. Pearl and M. C. Zerner, *J. Am. Chem. Soc.*, 1999, **121**, 399; K. K. Stavrev and M. C. Zerner, *J. Am. Chem. Soc.*, 1995, **117**, 8684.
84 P. C. Ford, *Coord. Chem. Rev.*, 1970, **5**, 75.
85 L. A. Pavanin, E. Giesbrecht and E. Tfouni, *Inorg. Chem.*, 1985, **24**, 4444.
86 A. Ohyoshi and K. Yoshikuni, *Bull. Chem. Soc. Jpn.*, 1979, **52**, 3105.
87 C. Hansch, A. Leo and R. W. Taft, *Chem. Rev.*, 1991, **91**, 165.
88 A. Szabo and N. S. Ostlund, *Modern Quantum Chemistry, Introduction to Advanced Electronic Structure Theory*, Dover Publications Inc., Mineola, New York, 1996, p. 85.